Electronic Supplementary Information for

Ordered Structures and Sub-5 nm Line Patterns from Rod−Coil Hybrids Containing Oligo(dimethylsiloxane)

Weilu Yang, Wei Zhang, Longfei Luo, Xiaolin Lyu, Anqi Xiao, Zhihao Shen,* and Xing-He Fan*

Beijing National Laboratory for Molecular Sciences, Key Laboratory of Polymer Chemistry and Physics of Ministry of Education, Center for Soft Matter Science and Engineering, and College of Chemistry and Molecular Engineering, Peking University, Beijing 100871, China

Table of contents

Experimental Section

Materials

4-Bromo-4'-hydroxybiphenyl (98%, Energy Chemical), 4-bromobut-1-ene (97%, Aladdin), 8-bromo-1-octene (98%, Energy Chemical), potassium carbonate (AR, Acros), Karstedt catalyst solution (Pt(dvs), Pt ~2% in Xylene, Energy Chemical), 1,8-diazabicyclo[5.4.0]undec-7-ene (98%, Adamas), copper (I) iodide (98%, Energy Chemical), bis(triphenylphosphine)palladium (II) chloride (98%, Innochem), 1,1,1,3,3,5,5-heptamethyltrisiloxane (90%, Adamas), hexamethylcyclotrisiloxane (98%, Energy Chemical), chlorodimethylsilane (95%, Energy Chemical), Pd/C (10% on carbon, TCI), sodium phosphate monobasic dehydrate (99%, Greagent), sodium phosphate dibasic dodecahydrate (99%, Greagent), 1,4-dioxane (99%, Sigma-Aldrich), and ethyl acetate (HPLC, J&K Chemical) were used as received. Dichloromethane (DCM, HPLC, J&K Chemical), toluene (HPLC, J&K Chemical), and acetone (HPLC, J&K Chemical) were purified using the M Braun SPS-800 solvent purification system. Other chemical reagents were commercially available and used without further purification.

Synthetic Procedures

The general synthetic routes of the intermediates **Si_3-C_4-Ph_2-Br**, **Si_7-C_4-Ph_2-Br**, **Si_{11}-C_4-Ph_2-Br**, and **Si_7-C_8-Ph_2-Br** are shown in Scheme S1. The synthesis of **Si_7-H** follows the procedure in Meijer *et al.*'s work.[1]

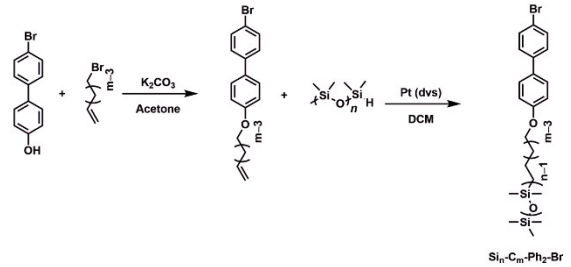

Scheme S1 Synthetic route of **Si_3-C_4-Ph_2-Br**, **Si_7-C_4-Ph_2-Br**, **Si_{11}-C_4-Ph_2-Br**, and **Si_7-C_8-Ph_2-Br**.

Synthesis of 4-Bromo-4'-(but-3-en-1-yloxy)-1,1'-biphenyl. 4'-Bromo-[1,1'-biphenyl]-4-ol (24.9 g, 100 mmol), 4-bromobut-1-ene (13.5 g, 200 mmol), and K_2CO_3 (27.6 g, 200 mmol)

were dissolved in 100 mL of acetone in a round-bottomed flask. Then the reaction mixture was stirred at 80 ^{o}C for 12 h. After acetone was removed under vacuum, the residue was dissolved in 100 mL of DCM and washed with 60 mL of deionized water for three times. The organic layer was collected and dried by anhydrous $MgSO_4$ for 30 min. And DCM was removed under a reduced pressure, and the crude product was purified by column chromatography (eluent: petroleum ether (PE)/DCM = 3:1, v:v) on silica gel to afford 22.4 g of 4-bromo-4'-(but-3-en-1-yloxy)-1,1'-biphenyl as a white powder. Yield: 74.1%. ^{1}H NMR (400 MHz, $CDCl_3$, δ, ppm): 7.65 (m, 4H), 7.63 (m, 2H), 6.99 (m, 2H), 5.82 (m, 1H), 5.13 (m, 1H), 4.88 (m, 1H), 3.98 (t, 2H), 2.38 (m, 2H).

Synthesis of 4-Bromo-4'-(oct-7-en-1-yloxy)-1,1'-biphenyl. The synthetic procedure of 4-bromo-4'-(oct-7-en-1-yloxy)-1,1'-biphenyl was similar to that of 4-bromo-4'-(but-3-en-1-yloxy)-1,1'-biphenyl. Yield: 62.0%. ^{1}H NMR (400 MHz, $CDCl_3$, δ, ppm): 7.47 (m, 6H), 6.96 (m, 2H), 4.96 (m, 1H), 3.99 (t, 1H), 3.41 (t, 2H), 2.06 (m, 2H), 1.82 (m, 2H), 1.54–1.30 (m, 6H).

Synthesis of Br-Ph$_2$-C$_4$-Si$_3$. 4-Bromo-4'-(but-3-en-1-yloxy)-1,1'-biphenyl (1.52 g, 5.00 mmol) and Me-Si_3-H (1.34 g, 6.00 mmol) were added to a 25 mL Schlenk flask and kept under a nitrogen atmosphere. Then 5 mL of DCM and two drops of Karstedt's catalyst (1% in xylene) were subsequently added through a syringe. The reaction mixture was stirred at ambient temperature overnight. After the reaction finished, 0.5 mL of methanol was added to quench the reaction. Then the organic solvent was removed by rotary evaporator. And the crude product was purified by column chromatography (eluent: PE/DCM = 3:1, v:v) to afford 1.89 g of Br-Ph_2-C_4-Si_3 as a pale yellow solid. Yield: 71.7%. ^{1}H NMR (400 MHz, $CDCl_3$, δ,

ppm): 7.47 (m, 6H), 6.96 (d, 2H), 4.00 (t, 2H), 1.84 (m, 2H), 1.49 (m, 2H), 0.61 (m, 2H), 0.09 (m, 15H), 0.03 (m, 6H).

Synthesis of Br-Ph$_2$-C$_4$-Si$_7$. The synthetic procedure of Br-Ph$_2$-C$_4$-Si$_7$ was similar to that of Br-Ph$_2$-C$_4$-Si$_3$. Yield: 72.4%. ^{1}H NMR (400 MHz, CDCl$_3$, δ, ppm): 7.47 (m, 6H), 6.96 (d, 2H), 4.00 (t, 2H), 1.83 (m, 2H), 1.53 (m, 2H), 0.61 (t, 2H), 0.11–0.02 (45H).

Synthesis of Br-Ph$_2$-C$_4$-Si$_{11}$. The synthetic procedure of Br-Ph$_2$-C$_4$-Si$_{11}$ was similar to that of Br-Ph$_2$-C$_4$-Si$_3$. Yield: 70.9%. ^{1}H NMR (400 MHz, CDCl$_3$, δ, ppm): 7.47 (m, 6H), 6.96 (d, 2H), 4.00 (t, 2H), 1.83 (m, 2H), 1.53 (m, 2H), 0.61 (t, 2H), 0.11–0.02 (69H).

Synthesis of Br-Ph$_2$-C$_8$-Si$_7$. The synthetic procedure of Br-Ph$_2$-C$_4$-Si$_{11}$ was similar to that of Br-Ph$_2$-C$_4$-Si$_3$. Yield: 100%. ^{1}H NMR (400 MHz, CDCl$_3$, δ, ppm): 7.47 (m, 6H), 6.96 (d, 2H), 3.99 (t, 2H), 1.80 (m, 2H), 1.53–1.22 (m, 10H), 0.54 (t, 2H), 0.11–0.02 (m, 45H).

The oligodimethylsiloxane (ODMS)-containing rod–coil LCs **Si$_3$-C$_4$-Rod**, **Si$_7$-C$_4$-Rod**, **Si$_{11}$-C$_4$-Rod**, and **Si$_7$-C$_8$-Rod** were synthesized in a similar way by Sonogashira coupling of bromide-terminated monodisperse ODMS as shown in Scheme S2.

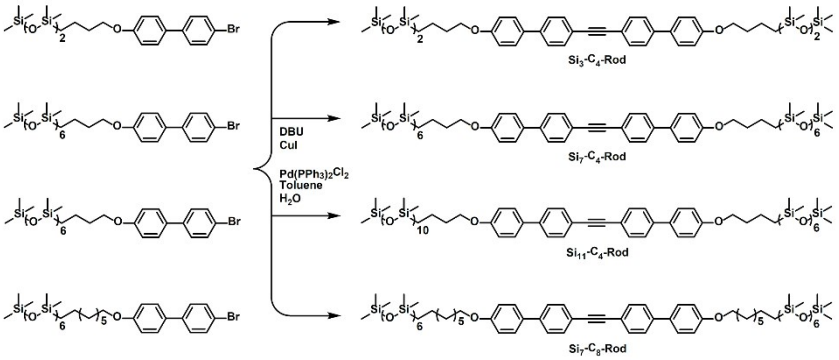

Scheme S2 Synthetic routes of **Si$_3$-C$_4$-Rod**, **Si$_7$-C$_4$-Rod**, **Si$_{11}$-C$_4$-Rod**, and **Si$_7$-C$_8$-Rod**.

Synthesis of Si$_3$-C$_4$-Rod. Si$_3$-C$_4$-Rod was synthesized by Sonogashira coupling reaction. Br-Ph$_2$-C$_4$-Si$_3$ (1.05 g, 2.00 mmol), bis(triphenylphosphine)palladium(II) chloride (84.0 mg,

0.120 mmol), and cuprous iodide (CuI, 38.0 mg, 0.200 mmol) were added into a Schlenk flask and kept under an Argon atmosphere. Then 5 mL of dry toluene was added through a syringe. After dissolution, trimethylsiloxane (0.140 mL, 1.00 mmol), 1,8-diazabicyclo[5,4,0]-undec-7-ene (DBU, 183 mg, 0.0840 mmol), and deionized water (0.0140 mL, 0.780 mmol) were added in sequence via a syringe. The reaction mixture was stirred at 60 ^{o}C for 18 h. After the reaction finished, the reaction mixture was washed with 60 mL of deionized water for 3 times, and the organic layer was collected and dried with anhydrous $MgSO_4$. The crude product was collected by removing the organic solvent under a reduced pressure and was purified by column chromatography (eluent: petroleum ether (PE)/dichloromethane (DCM) = 6:1, v:v) on silica gel to afford 302 mg of Si_3-C_4-Rod as a light yellow waxy solid. Yield: 33.0%. ^{1}H NMR (400 MHz, $CDCl_3$, *δ*, ppm): 7.56 (m, 12H), 6.98 (d, 4H), 4.01 (t, 4H), 1.84 (m, 4H), 1.53 (m, 4H), 0.62 (t, 4H), 0.11–0.02 (m, 42H). ^{13}C NMR (125 MHz, $CDCl_3$, δ, ppm):159.3, 140.90, 132.90, 132.27, 128.29, 126.77, 121.80, 115.17, 90.20, 68.03, 37.41, 20.11, 18.29, 2.13, 1.58, 0.49. MALDI-TOF MS: $[M + H]^+$/z, Calcd., 915.62; Found, 914.48.

Synthesis of Si_7-C_4-Rod. The synthetic procedure of Si_7-C_4-Rod was similar to that of Si_3-C_4-Rod. Yield: 30.8%. ^{1}H NMR (400 MHz, $CDCl_3$, *δ*, ppm): 7.55 (m, 12H), 6.97 (m, 4H), 4.01 (t, 4H), 1.84 (m, 4H), 1.55 (m, 4H), 0.62 (t, 4H), 0.11–0.02 (m, 90H). ^{13}C NMR (125 MHz, $CDCl_3$, δ, ppm): 141.5, 140.5, 138.0, 132.8, 130.1, 129.2, 127.7, 121.6, 89.7, 35.4, 34.4, 23.9, 19.6, 6.2, 5.8, 5.3. MALDI-TOF MS:$[M + H]^+$/z, Calcd., 1508.86; Found, 1508.62.

Synthesis of Si_{11}-C_4-Rod. The synthetic procedure of Si_{11}-C_4-Rod was similar to that of Si_3-C_4-Rod. Yield: 33.5%. ^{1}H NMR (400 MHz, $CDCl_3$, *δ*, ppm): 7.54 (s, 12H), 6.97 (d, 4H), 4.01 (t, 4H), 1.84 (m, 4H), 1.55 (m, 4H), 0.62 (t, 4H), 0.11–0.02 (m, 138H). ^{13}C NMR (125 MHz,

$CDCl_3$, δ, ppm): 159.47, 141.84, 133.14, 132.52, 132.20, 128.28, 128.22, 126.78, 126.71, 120.08, 115.14, 115.09, 82.15, 77.55, 77.23, 76.91, 74.71, 67.96, 33.01, 20.02, 18.19, 2.01, 1.65, 1.41, 1.37, 1.31, 1.28, 0.91, 0.41, 0.22. MALDI-TOF MS:$[M + H]^+$/z, Calcd., 2102.09; Found, 2101.64.

Synthesis of Si_7-C_8-Rod. The synthetic procedure of Si_7-C_8-Rod was similar to that of Si_3-C_4-Rod. Yield: 32.3%. ^{1}H NMR (400 MHz, $CDCl_3$, δ, ppm): 7.54 (m, 12H), 6.98 (d, 4H), 4.28 (t, 4H), 4.00 (t, 4H), 1.81 (m, 4H), 1.50–1.23 (m, 10H), 0.54 (m, 4H), 0.11–0.02 (m, 90H). ^{13}C NMR (125 MHz, $CDCl_3$, δ, ppm): 141.82, 133.14, 132.52, 128.28, 126.77, 120.07, 115.14, 77.55, 77.23, 76.91, 68.36, 33.62, 29.59, 29.55, 29.51, 26.32, 23.44, 18.49, 2.02, 1.41, 1.38, 1.30, 0.42, 0.22. MALDI-TOF MS:$[M + H]^+$/z, Calcd., 1621.07; Found, 1621.01.

Instrumentation and Characterization

^{1}H and ^{13}C NMR spectra were acquired by a Bruker-400 (400 MHz) spectrometer with $CDCl_3$ solvent. The determination of chemical displacement (ppm) was based on the internal standard of tetramethylsilane (TMS). The chemical shift of $CDCl_3$ was 7.27 ppm in ^{1}H NMR spectra and 77.00 ppm in ^{13}C NMR spectra. Matrix-assisted laser desorption/ionization time-of-flight (MALDI-TOF) mass spectrometry was performed on a AB Sciex 5800 MALDI-TOF spectrometer using 2,5-dihydroxybenzoic acid (DHB) matrix. Thermogravimetric analysis (TGA) were carried out on a Q600 SDT analyzer under N_2 gas with a flow rate of 100 mL min^{-1} and a heating rate of 10 °C min^{-1} from ambient temperature to 600 °C. Differential scanning calorimetry (DSC) experiments were carried out on a Q100 DSC calorimeter under N_2 atmosphere with a flow rate of 50 mL min^{-1} and a scanning rate of 10 °C min^{-1} during both the heating and cooling processes. The data of the first cooling and

the second heating process were recorded. Polarized light microscopy (PLM) experiments were carried out on a Nikon DS-Ril microscopy with an Instec HCS302 hot stage. A small amount of sample was placed on a glass slide and pressed into a thin film with cover glass for testing. The temperature was first raised so that the sample was in the isotropic state, and then the texture changes were observed during the cooling process. Wide-angle X-ray scattering (WAXS) profiles and grazing-incidence wide-angle X-ray diffraction (GI-WAXD) patterns were acquired using Ganesha SAXS produced by SAXS LAB. The wavelength of the X-ray is 0.154 nm. Cross-section scanning electron microscopy (SEM) image of thin film was taken using Hitachi S-4800 cold-field emission scan electron microscopy. Atomic-force microscopy (AFM) images were recorded in the tapping mode under ambient conditions using a NanoScope Analysis 1.5 Atomic force microscope fitted with a silicon probe (Bruker, RTESP, spring constant 42 N/m and a resonance frequency 320 kHz).

Preparation of Thin Films

The silicon substrate was decorated with a polydimethylsiloxane (PDMS) brush by hydrophilic modification and PDMS modification. A heptane solution of 1.5 wt% hydroxyl-terminated PDMS homopolymer (M_n = 5000 Da) was coated onto the hydrophilically modified Si wafer at 3000 rpm for 45 s and baked at 150 °C for 24 h. The thickness of the grafted PDMS polymer brush layer was estimated to be 3−4 nm according to C. A. Ross's publication.[2] After that, 1 wt% heptane solution of each sample was coated onto a modified silicon wafer at 3000 rpm for 60 s, respectively.

Results

Table S1 Thermal transition data of **Si_3-C_4-Rod, Si_7-C_4-Rod, Si_{11}-C_4-Rod, and Si_7-C_8-Rod**.[a]

Sample	First cooling	Second heating
Si_3-C_4-Rod	**Iso**–163–**Lam**–135–**K-in-Lam**	**K-in-Lam**–139–**Lam**–161–**Iso**
Si_7-C_4-Rod	**Iso**–123–**Gyr**–75–**K-in-Gyr**	**K-in-Gyr**–81–**Gyr**–121–**Iso**
Si_{11}-C_4-Rod	**Iso**–128–**Col_r-II**–67–**Col_r-I**	**Col_r-I**–73–**Col_r-II**–127–**Iso**
Si_7-C_8-Rod	**Iso**–166–**Col_h**	**Col_h**–166–**Iso**

[a] Phase transition temperatures (°C), K-in-Lam = coexisting lamellae-crystal, Lam = lamellae, K-in-Gyr = coexisting gyroid-crystal, Gyr = gyroid, Col_r-I = rectangular columnar at relatively lower temperatures, Col_r-II = rectangular columnar at relatively higher temperatures, Col_h = hexagonal columnar, Iso = isotropic.

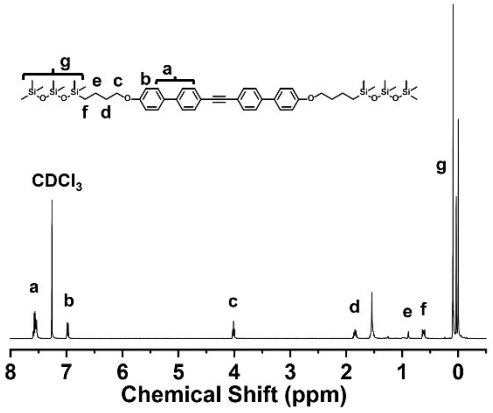

Fig. S1 ^{1}H NMR spectrum of **Si_3-C_4-Rod**.

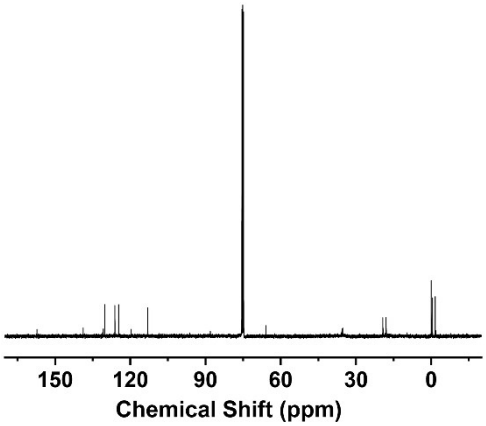

Fig. S2 ^{13}C NMR spectrum of **Si$_3$-C$_4$-Rod**.

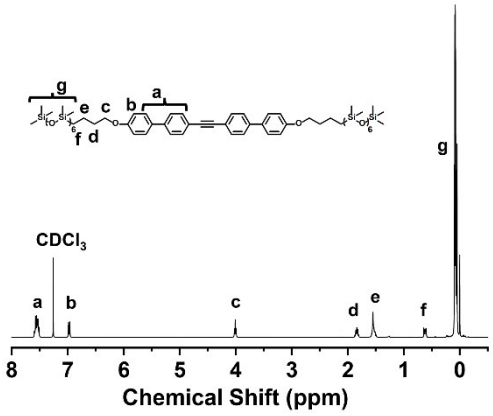

Fig. S3 ^{1}H NMR spectrum of **Si$_7$-C$_4$-Rod**.

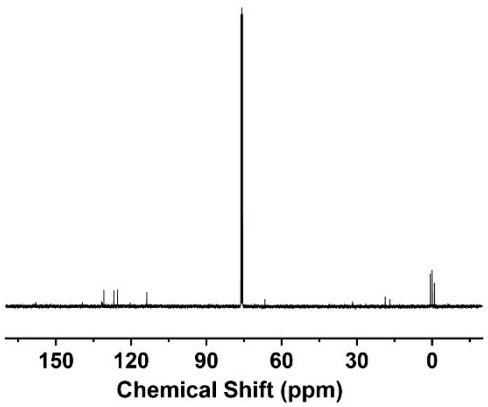

Fig. S4 ^{13}C NMR spectrum of **Si$_7$-C$_4$-Rod**.

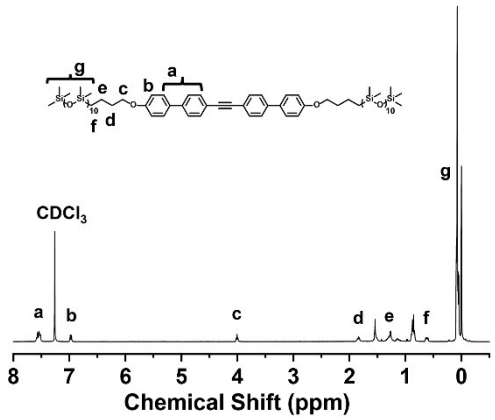

Fig. S5 ^{1}H NMR spectrum of **Si_{11}-C_4-Rod**.

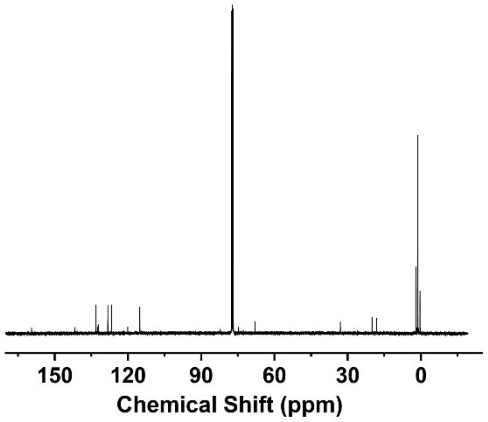

Fig. S6 ^{13}C NMR spectrum of **Si_{11}-C_4-Rod**.

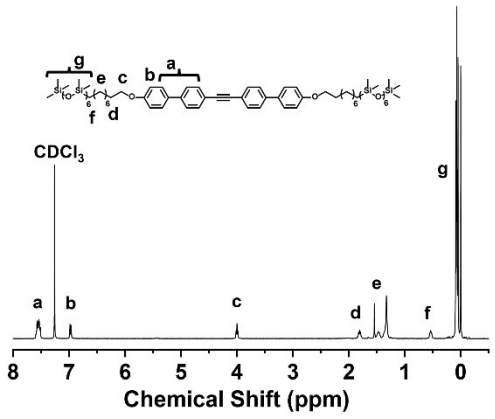

Fig. S7 ^{1}H NMR spectrum of **Si_7-C_8-Rod**.

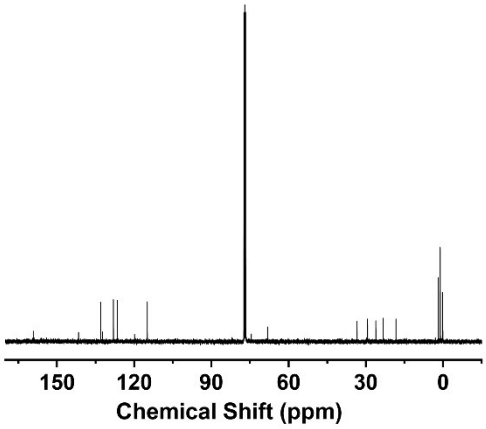

Fig. S8 ^{13}C NMR spectrum of **Si_7-C_8-Rod**.

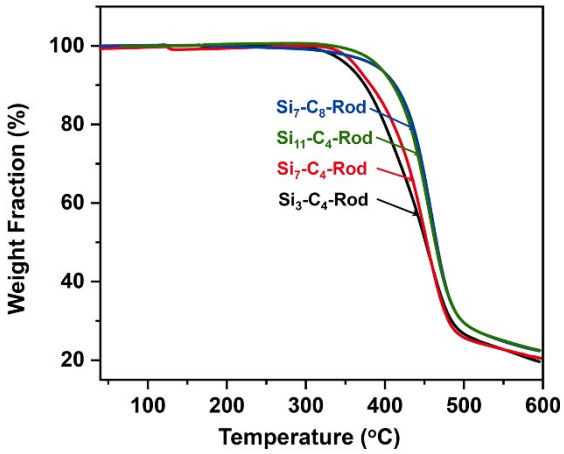

Fig. S9 TGA curves of **Si_3-C_4-Rod**, **Si_7-C_4-Rod**, **Si_{11}-C_4-Rod**, and **Si_{11}-C_4-Rod** at a rate of 10 °C min^{-1} under a nitrogen atmosphere.

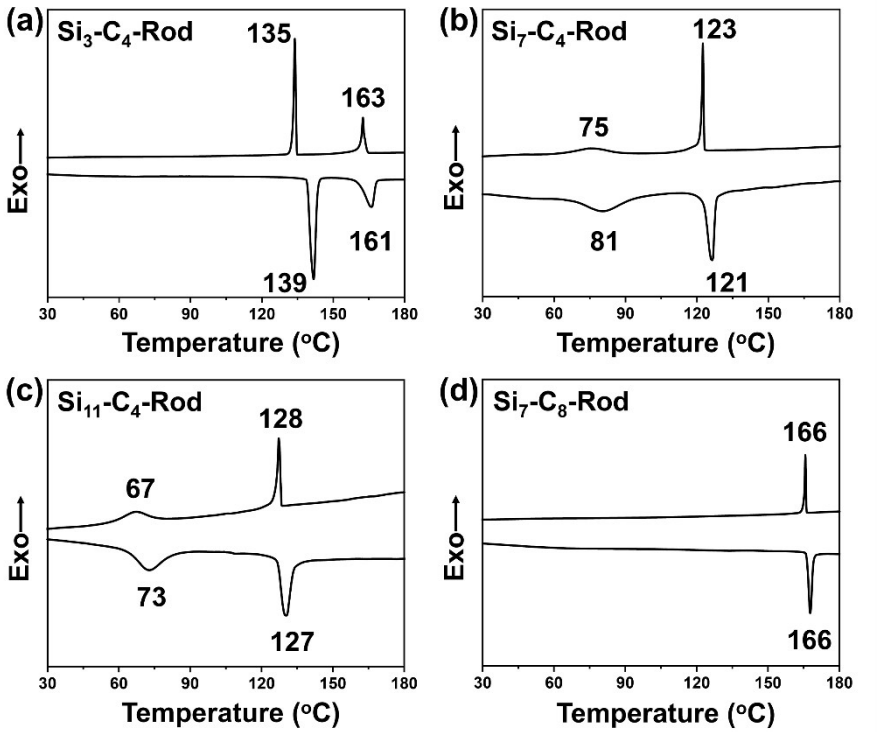

Fig. S10 DSC first-cooling and second-heating curves of **Si_3-C_4-Rod** (a), **Si_7-C_4-Rod** (b), **Si_{11}-C_4-Rod** (c), and **Si_7-C_8-Rod** (d) at a rate of 10 °C min^{-1} under nitrogen atmosphere. Phase transition temperatures (°C) are marked.

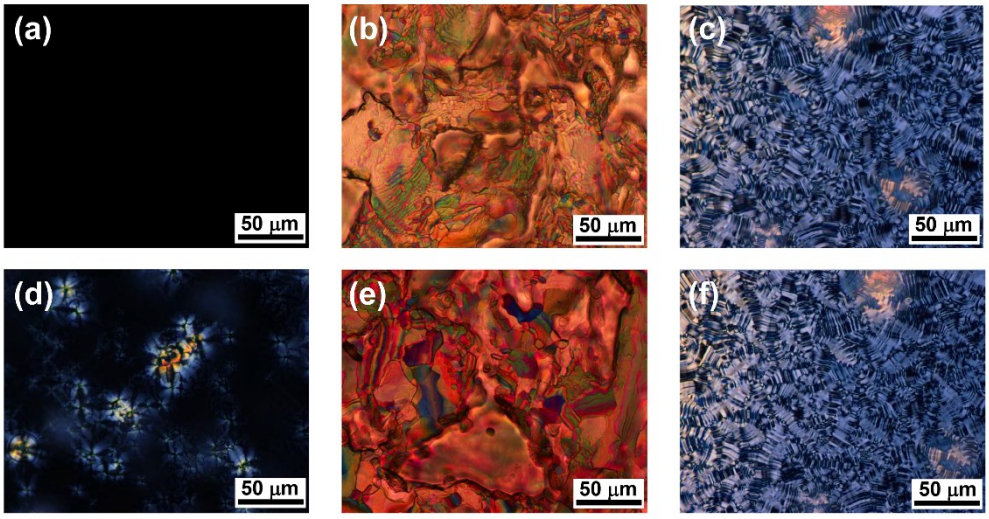

Fig. S11 PLM micrographs of LCs at 180 °C (a); PLM micrographs of **Si_3-C_4-Rod** at 30 °C (b); PLM micrographs of **Si_{11}-C_4-Rod** at 30 °C (c); PLM micrographs of **Si_7-C_8-Rod** at 30 °C (d); PLM micrographs of **Si_3-C_4-Rod** at 150 °C (e) and **Si_{11}-C_4-Rod** at 100 °C (f).

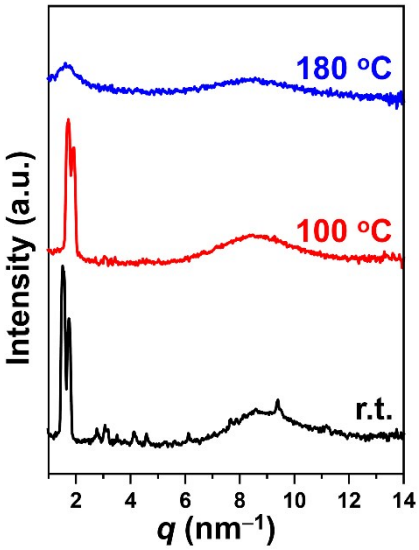

Fig. S12 Temperature-dependent WAXS profiles of **Si_7-C_4-Rod**.

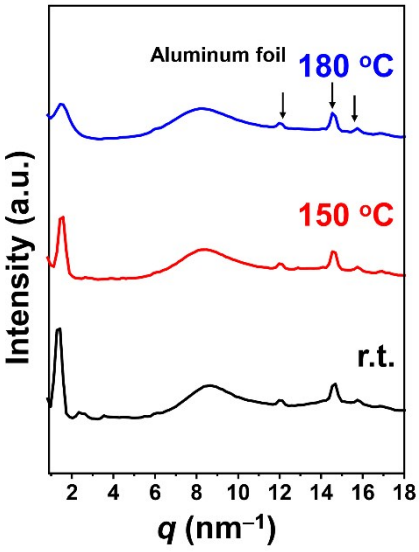

Fig. S13 Temperature-dependent WAXS profiles of **Si_{11}-C_4-Rod** (the three peaks marked by arrows are attributed to the diffractions of aluminum foil during testing).

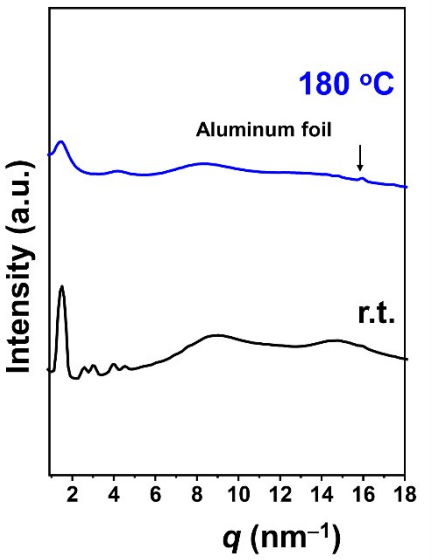

Fig. S14 Temperature-dependent WAXS profile of **Si_7-C_8-Rod** (the peak marked by arrow is attributed to the diffractions of aluminum foil during testing).

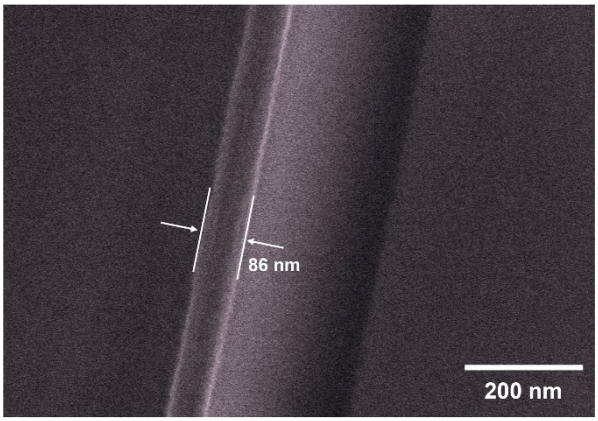

Fig. S15 Cross-sectional SEM image of a thin film of **Si_{11}-C_4-Rod**.

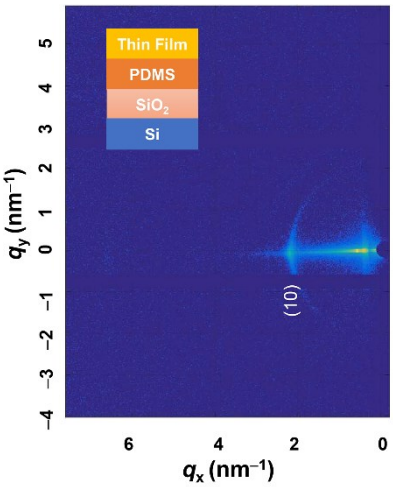

Fig. S16 GI-WAXD pattern of **Si_3-C_4-Rod**.

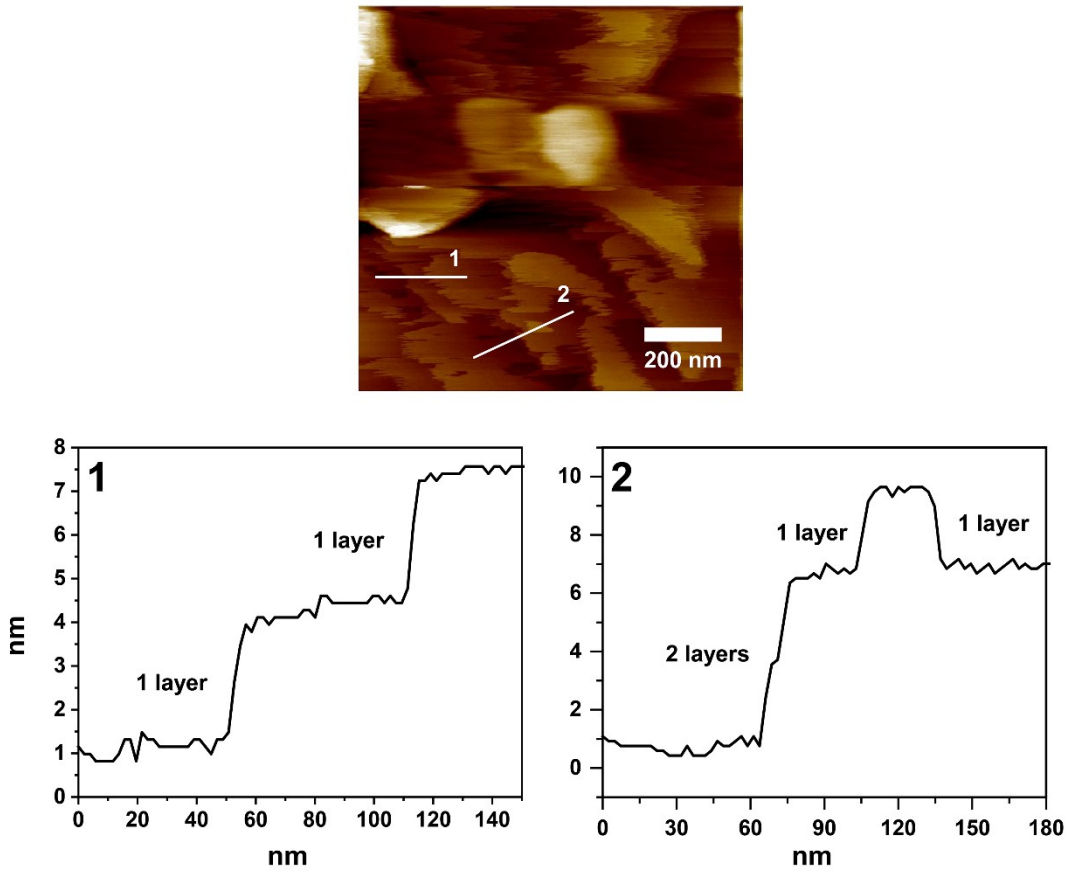

Fig. S17 AFM height image (top) and cross-sectional curves (bottom) of **Si_3-C_4-Rod**.

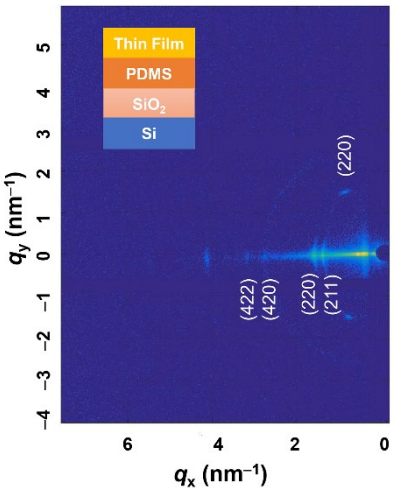

Fig. S18 GI-WAXD pattern of **Si_7-C_4-Rod**.

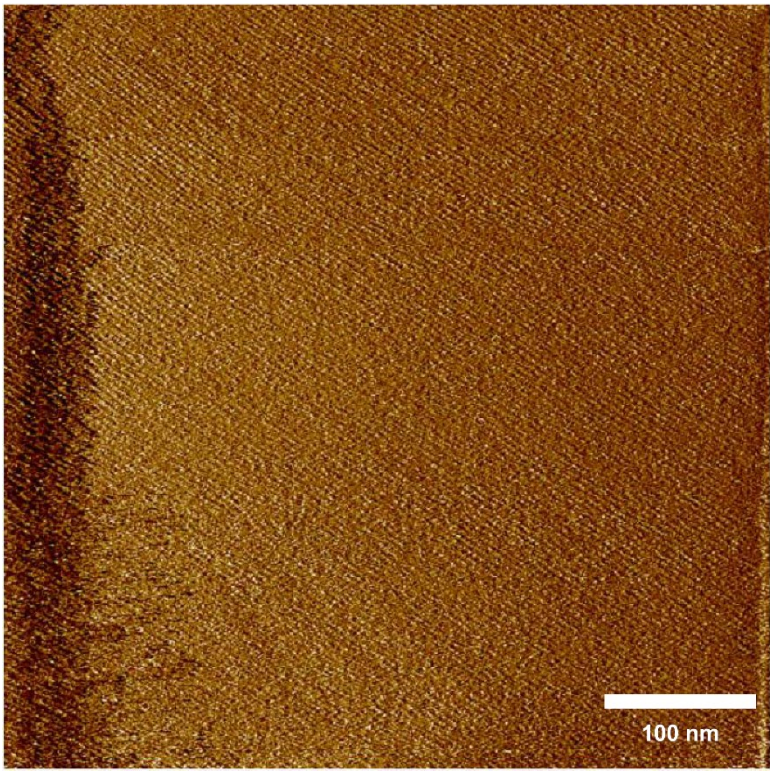

Fig. S19 Large-area AFM image of **Si_7-C_4-Rod**.

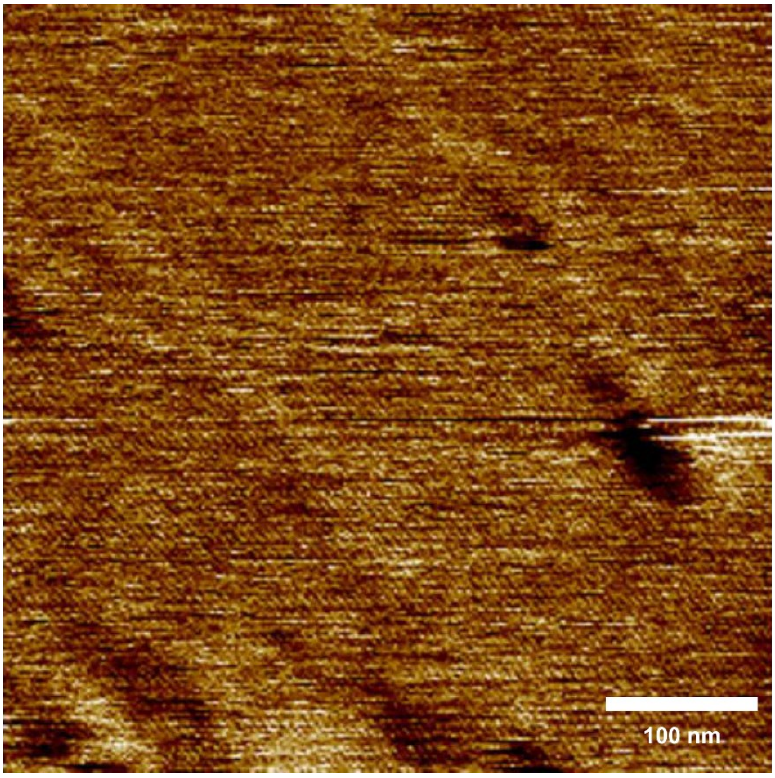

Fig. S20 Large-area AFM image of **Si_{11}-C_4-Rod**.

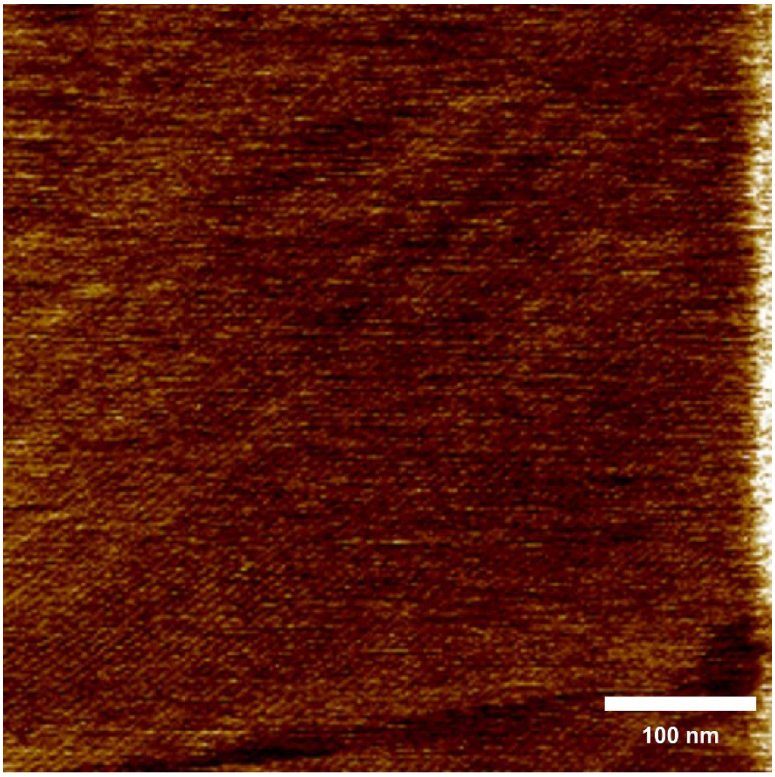

Fig. S21 Large-area AFM image of **Si_7-C_8-Rod**.

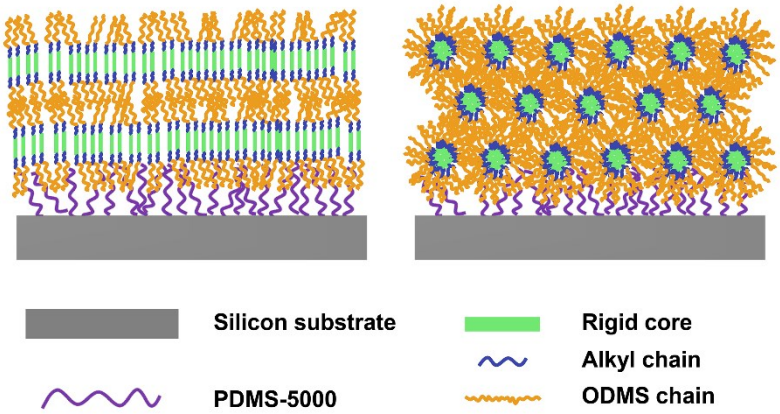

Fig. S22 Schemetic models of the molecular alignment at the interfaces when the rod–coil molecule is in the lamellar (upper left part) and columnar (upper right part) phases.

References:

1. B. van Genabeek, B. F. M. de Waal, M. M. J. Gosens, L. M. Pitet, A. R. A. Palmans and E. W. Meijer, *J. Am. Chem. Soc.*, 2016, **138**, 4210-4218.
2. Y. S. Jung and C. A. Ross, *Nano Lett.*, 2007, **7**, 2046-2050.